Morphologies from slippery ballistic deposition model: A bottom-up approach for nanofabrication

Anthony Robledo,[1] Christopher N. Grabill,[2] Stephen M. Kuebler,[1,2,3] Aniruddha Dutta,[1]
Helge Heinrich,[1,4] and Aniket Bhattacharya[1,*]

[1]*Department of Physics, University of Central Florida, Orlando, Florida 32816-2385, USA*
[2]*Department of Chemistry, University of Central Florida, Orlando, Florida 32816-2385, USA*
[3]*CREOL, College of Optics and Photonics, University of Central Florida, Orlando, Florida 32816-2385, USA*
[4]*AMPAC, University of Central Florida, Orlando, Florida 32816-2385, USA*

(Received 1 October 2010; revised manuscript received 10 February 2011; published 13 May 2011)

We report pattern formation using a slippery ballistic deposition (SBD) model where growth germinates from a single site or from sites distributed periodically on a lattice. By changing the sticking probability p_s and choosing systems with different lattice constants and symmetries, we demonstrate that a variety of patterns can be generated. These patterns can be further used as scaffolds for nanofabrication. We also demonstrate that by choosing a lateral sticking probability p_l at the base that is different than p_s, one can control both the early and late time morphologies originating from a seed. Furthermore, we indicate a possible generalization of preparing patterns to higher dimensions that in principle can have potential technological applications for preparing grooves and scaffolds of specific shapes and periodicities.

DOI: 10.1103/PhysRevE.83.051604 PACS number(s): 81.15.Aa, 68.35.Ct, 68.55.−a, 05.50.+q

I. INTRODUCTION

The deposition of particles onto various soft and hard surfaces is a matter of broad general interest in physics, chemistry, biology, and engineering because of their immense practical importance [1]. Typically many of these processes are characterized by evolving rough surfaces, e.g., in a flame, epitaxial growth, or electro- and electroless depositions. There is an active region that grows, and, therefore, these systems intrinsically are far from equilibrium and pose many fundamental questions and challenges in describing these phenomena. The well-known Kardar-Parisi-Zhang (KPZ) equation [2] and Kuramoto-Sivashinsky equation [3] are examples of description of such nonequilibrium phenomena in terms of differential equations involving space and time [1]. Naturally, considerable interest has developed in studying evolving growth morphologies at various length and time scales under nonequilibrium conditions over the last three decades. In an effort to understand the fundamental nature of the growth processes, their universal aspects, as well as detail short length scale structures of the evolving morphologies, various models have been developed with a prescribed set of rules mostly for lattices in one and two spatial dimensions. Random deposition (RD) and ballistic deposition (BD) models, the diffusion limited aggregation (DLA) model [4], the Eden model [5], and the random sequential adsorption (SRA) model [6], to name a few, were inspired by and designed to model specific phenomena. For example, RD and BD models have been studied in detail in one and two dimensions in the context of molecular beam epitaxy. Likewise, the Eden model was introduced to study growth of tumor cells, and DLA and its variants have been studied to understand shoots, colloids, and snowflakes. SRA models were introduced to understand adsorption of proteins on surfaces. Despite the fact that a vast amount of theoretical work validated by numerical work has been accomplished, with more accurate microscopy and refined tomographic techniques capable of probing inhomogeneities at much shorter length scales, the nonequilibrium growth phenomena continues to offer intriguing questions.

The BD model is one of the simplest models among those mentioned above, independently introduced by Vold [7] and Sutherland [8] originally to study the sedimentation phenomena of colloidal particles. But in recent years the interest in studying the BD model has shifted to understand the growth of films [9,10]. This model has been studied numerically in one spatial dimension as well as in two spatial dimensions, mainly numerically. In the literature this is usually referred to as $(1+1)$ dimensions (2D) and $(2+1)$ dimensions (3D), considering growth direction (time) as another dimension. But in our studies we will refer to growth in one and two spatial dimensions as one and two dimensions, respectively. In the regular BD model the sticking probability p_s is considered to be unity. One can generalize the rules for random deposition by varying the sticking probability to be less than unity. This generalization can be continued even further where one assigns a different probability at the base surface from where the pattern begins to grow. Evidently these generalizations will result in patterns whose local structures and universal aspects are worthy of investigation.

The primary objective of this paper is to study growth patterns in a SBD model. In particular, our focus is to look at patterns that can be generated from a *single seed* by varying the sticking probability alone. Then we extend this idea for a periodic lattice. Indeed, we find that in addition to varying the sticking probability, one can obtain patterns by exploiting the symmetry of the lattice and varying the length of the primitive basis vectors. We believe that if this idea demonstrated through computer simulations can be translated to real experiments, it will open the door for routes to templating and scaffolding at very small length scales. We also generalize this idea and demonstrate with a few examples how these patterns change as the lateral sticking probability p_l at the bottom is changed.

While exploring patterns in a SBD model, as a by-product we carry out simulation in the bulk for the regular BD model for reasonably large lattices. Although studied quite exhaustively, the connection between the BD model and the KPZ equation

*aniket@physics.ucf.edu

has been revisited by a number of authors recently. We briefly present some results for the regular BD model obtained from lattice sizes 2^6–2^{13}. This also allows us to test and benchmark the numerical results in the range where they have been well studied.

Motivated by experiments in which gold nanoparticles are used to nucleate electroless deposition of silver onto polymeric surfaces [11], we have undertaken the task of analyzing the evolving morphologies as a function of time and distance from the substrate where the impurities or nanoparticles reside. The BD model may not be strictly justified for electroless deposition; however, these studies complemented by studies of diffusive growth models will then guide us to develop better microscopic understanding of the fundamental processes involved. The rest of the paper is organized as follows. In the following section we describe the BD model. In Sec. III we summarize our results. We conclude in Sec. IV with a discussion and possible generalization and extension of the ideas reported here for future work.

II. BALLISTIC DEPOSITION MODEL

The simplest version of the lattice BD model [1] in one dimension is as follows. From a lattice of length L a column position i $(0 \leqslant i \leqslant L)$ is chosen at random. A particle is allowed to travel vertically downward along the ith column until it gets adsorbed at a height $h(i,n+1)$ at a discrete time $n+1$ determined by the following rule:

$$h(i,n+1) = \mathrm{Max}[h(i-1,n),h(i,n),h(i+1,n)], \qquad (1)$$

where $h(i,n)$, $h(i \pm 1,n)$ are the heights of the column i and the heights of its nearest neighbor columns $i \pm 1$, respectively, and the operation "Max" corresponds to the maximum of these three heights. Therefore, the BD is model is completely specified by the function $h(\{\mathbf{r}_i\},n)$, where $\mathbf{r}_i$ represents the position of the maximum height of the ith column in general. The interesting physical quantity is not the mean height $\bar{h}$, (which according to the prescribed rule grows linearly with time) but the fluctuation of the interface width $\xi(L,t)$ at time t (height fluctuation) defined as

$$\xi(L,t)^2 = \frac{1}{L}\sum_{x=1}^{L}[h(x,t) - \bar{h}(t)]^2. \qquad (2)$$

Typically kinetics of rough surfaces are characterized by the dynamical scaling of a growing correlation [12]. In the BD model this quantity is the height-height correlation manifested in the height fluctuation $\xi(L,t)$. At early time the interface is characterized by the growth exponent β defined as $\xi \sim t^{\beta}$, while at late time the fluctuation of the interface saturates and is described by the roughness exponent α, for which $\xi_{\mathrm{sat}} \sim L^{\alpha}$. The early and late time behavior is quantified by the nonequilibrium z exponent, such that at a characteristic time t_x the height fluctuation $\xi(L,t_x) \sim L$ and is described as $t_x \sim L^{1/z}$ [12]. Therefore, early and late time implies $t \ll t_x$ and $t \gg t_x$ respectively. According to the dynamical scaling ansatz, first proposed for the BD model by Family and Vicsek [13], the height fluctuation $\xi(L,t)$ is described by the following equation:

$$\xi(L,t) = L^{\alpha} f(t/L^z). \qquad (3)$$

Since $f(x) \sim x^{\beta}$ for $x \ll 1$ and $f(x) \to \mathrm{const}$ for $x \gg 1$, from Eq. (3) it immediately follows that $z = \alpha/\beta$ [1]. Therefore, if this ansatz is obeyed, the height fluctuation scaled by L^{α} when plotted as a function of scaled time t/L^z should collapse onto a single master plot. Since for $t/L^z \gg 1$, $f(t/L^z) \to \mathrm{const}$, from Eq. (3) we note that in this limit $\xi(L) \sim L^{\alpha}$. Therefore, by measuring the saturation value of the $\xi(L,t \to \infty)$, one can systematically calculate the roughness exponent $\alpha(L)$ as a function of increasing lattice size L and extrapolate its asymptotic value for $L \to \infty$.

In one dimension, the KPZ equation can be exactly solved with $\alpha = 1/2$ and $\beta = 1/3$. Earlier simulation studies on the one-dimensional (1D) BD model up to $L = 2048$ in one dimension [14,15] reported smaller values of the exponent. D'Souza and collaborators [16,17] indicated that corrections to the scaling ansatz might be necessary. They have also indicated that correlation in the random number generator could be the cause of the discrepancy. This issues has been addressed in more recent simulation studies by Reis [18], who studied a 1D lattice up to 16 384 (2^{14}) and concluded from analysis for correction to scaling that $\alpha = 1/2$ and $\beta = 1/3$. Reis has also extended his 1D studies to investigate universality in two-dimensional (2D) KPZ growth using the BD model [19]. Furthermore, recently an exact lattice Langevin equation for the BD model has been derived by Haselwandter and Vvedensky [20]. The continuum limit of this equation has been shown to be dominated by the KPZ equation at all length and time scales. The 1D Langevin equation yields the KPZ scaling exponents, which prove beyond doubt that 1D KPZ and BD model share same universal aspects. Simulation studies of the BD model have also been extended for binary mixtures in one and two dimensions [21–23].

One of the important aspects to getting the asymptotic value of the exponents α and β is to run the simulation not only for large lattice sizes but also deep into the saturation regime. In his studies Reis [18] did not, however, run the simulation at the saturation regime for the two largest lattice sizes, $L = 8192$ and 16 384. We, on the contrary, have carried out simulation for lattice size up to 8192 but deep inside the saturation regime in one dimension and have concluded that exponents $\alpha = 0.5$ and $\beta = 1/3$ in a straightforward manner just by measuring the saturation values for several large lattice sizes, as shown in the next section.

III. SIMULATION RESULTS

Our Monte Carlo simulations involve both 1D and 2D lattices. It is worthwhile to note that with increasing lattice size the deposition time goes up considerably in order to get deep into the asymptotic limit (Fig. 1). Most of the results reported here are averaged over 1000 independent simulations. For 1D simulations we have simulated lattice sizes up to 2^{13} with a maximum number of 2^{31} deposited particles. For 2D simulations the maximum size was 1024×1024. The simulations

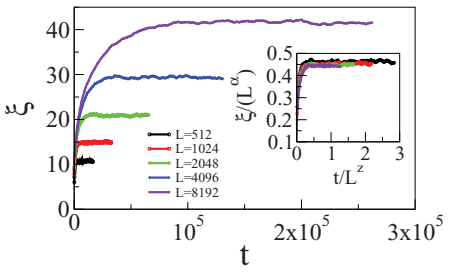

FIG. 1. (Color online) 1D ballistic growth in the bulk for lattice sizes $L = 512$, 1024, 2048, 4096, and 8192. The inset shows the scaled plots.

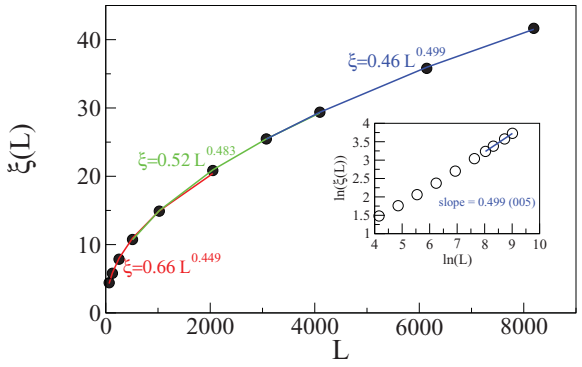

FIG. 2. (Color online) The height fluctuation $\xi(L,t \to \infty)$ (black circles) as a function of lattice size $L = 32$–8192. The red line is a fit to the data using lattice sizes $L = 32$–2048 described by the equation $\xi = (0.66 \pm 0.05)L^{0.449\pm0.008}$. The green line is described by $\xi = (0.52 \pm 0.02)L^{0.484\pm0.003}$ using the points $L = 256$–3072. The blue line is described by $\xi = (0.46 \pm 0.04)L^{0.499\pm0.005}$ using the points $L = 3072$–8192. The inset shows the corresponding log-log plot and the straight line (blue) corresponds to the slope 0.499 ± 0.005.

were carried out on three quad-core machines, which required approximately 30 days of uninterrupted simulation.

A. Bulk properties of 1D BD model

We have used the same random number generator as used by D'Souza [16] and simulated lattice sizes from 16 to 8192 in one dimension. For the sake of clarity, in Fig. 1 we show the height fluctuation for only the five largest lattice sizes. The same data are shown at the inset but with the height fluctuation scaled by L^{α} and the time scaled by L^{z}. For the largest two lattice sizes we observe excellent data collapse, while for smaller lattices slight deviations are noticeable due to finite size effects. In order to extract the exponents α and β we have used the following strategy. A little thought on the dynamical scaling aspect reveals that it is profitable to calculate the α exponent first from the late time data for $\xi(L,t)$ from the saturated regime. One notices from Fig. 1 that the saturated value of $\xi(L,t \to \infty)$ can be measured quite accurately. Therefore, we use the following equation:

$$\tilde{\alpha}(L,2L) = \frac{1}{\ln(2)} \ln \frac{\xi(2L,t \to \infty)}{\xi(L,t \to \infty)} \tag{4}$$

to calculate $\tilde{\alpha}(L,2L)$ from two successive lengths L and $2L$, and hence extract its asymptotic value as $L \to \infty$. Here we have used a separate notation $\tilde{\alpha}(L,2L)$ to emphasize that $\alpha(L)$ is calculated from the data obtained for lattice sizes L and $2L$, respectively, and hereafter will assume $\alpha(L) \equiv \tilde{\alpha}(L,2L)$.

The calculated values of $\alpha(L)$ extracted from successive pairs of lengths using Eq. (4) are shown in Table I. It is clear from the data that that the exponent α systematically increases toward the value $\frac{1}{2}$. It is worth mentioning that previous simulation by Meakin *et al.* [14] reported similar data for lattice size up to $L = 2048$. The height fluctuations listed in Table I are plotted in Fig. 2. Our values up to $L = 2048$ are almost exactly the same as those obtained by Meakin *et al.* Extending these simulation up to $L = 8192$, we obtain the asymptotic value of $\alpha = \frac{1}{2}$.

While calculating the β exponent we have taken a slightly different route than previously reported by Meakin *et al.* [14]. Since β is extracted from the early time behavior of $\xi(L,t)$, Meakin *et al.* used a very wide strip $L = 2^{18}$ and ran the simulation for shorter time. We calculate the z exponent instead and find it gives expected values in the large L limit. For each pair of lengths we used $\alpha(L,2L)$ and varied the z exponent to rescale time $t \to t/L^{z}$ to obtain the best data collapse and repeated the procedure for all the length pairs to get $z(L,2L)$. Hence we obtain β from $\beta(L,2L) = \tilde{\alpha}(L,2L)/z(L,2L)$. This procedure is shown in Fig. 3, where we show $\xi(L,t)/L^{\alpha}(L)$ as a function of time t. The corresponding inset shows a fine-tuned z exponent such that $\xi(L,t)/L^{\alpha}(L)$ versus t/L^{z} for lattice sizes L and $2L$ collapses on the same master plot. Evidently $z(L,2L)$ is size dependent, but we notice that the deviation from the sum rule $\alpha + z = 2.0$ [1] is within a small error bar for lengths $L = 512$–8192, and the dynamical scaling is also well obeyed for the data obtained for larger lattices. Our simulation data are completely consistent with more recent simulations studies for large system size by Reis [18] and

TABLE I. Asymptotic height fluctuation in the limit $t \gg L^{z}$, α, and β as a function of lattice size L.

L	$\xi(L) \pm \Delta\xi$	α	z	$\alpha + z$	β
64	4.414 ± 0.031				
128	5.807 ± 0.036	0.398 ± 0.002	1.31 ± 0.01	1.71 ± 0.01	0.31 ± 0.01
256	7.856 ± 0.052	0.433 ± 0.003	1.51 ± 0.01	1.95 ± 0.01	0.29 ± 0.01
512	10.747 ± 0.089	0.450 ± 0.002	1.515 ± 0.007	1.96 ± 0.01	0.30 ± 0.01
1024	14.901 ± 0.118	0.471 ± 0.008	1.535 ± 0.007	2.00 ± 0.01	0.310 ± 0.008
2048	20.850 ± 0.142	0.489 ± 0.002	1.566 ± 0.005	2.050 ± 0.008	0.320 ± 0.007
4096	29.384 ± 0.170	0.491 ± 0.002	1.545 ± 0.005	2.030 ± 0.005	0.320 ± 0.005
8192	41.641 ± 0.266	0.504 ± 0.001	1.560 ± 0.005	2.060 ± 0.005	0.320 ± 0.005

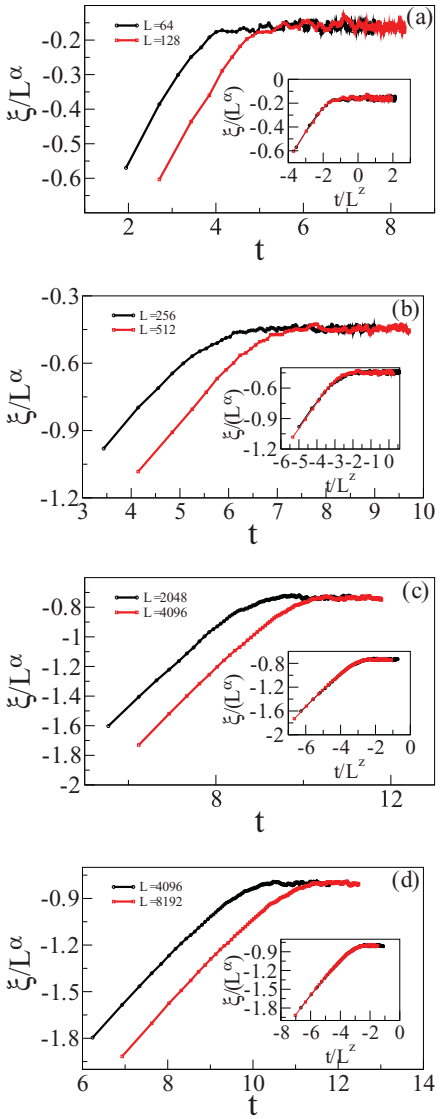

FIG. 3. (Color online) Scaled height fluctuations $\xi(L,t)/L^{\alpha}$ as a function of time for lattice sizes L and $2L$ using the value for α obtained using Eq. (3) as listed in Table I; (a) $L = 64$ and 128, (b) $L = 256$ and 512, (c) $L = 2048$ and 4096, and (d) $L = 4096$ and 8192. The inset demonstrates the best data collapse with rescaled time axis t/L^{z}. This value of the z exponent that corresponds to this "best" data collapse is listed in Table I.

with those obtained from lattice Langevin simulation results by Haselwandter and Vvedensky [20].

B. Height fluctuations without the voids

We now describe a "Gedanken" experiment that is relevant to characterizing morphology by transmission electron microscopy (TEM). It is noteworthy that the difference between RD and BD is that in the BD model lateral correlations among successive columns build up over time. This correlation is inherent to the BD growth. Consequently the height fluctuations in the BD model saturate when $\xi \sim L$, whereas ξ increases indefinitely in RD. Electrons in a TEM are not attenuated by voids. Therefore, imagine a situation in which an electron beam incident normal to a substrate passes through

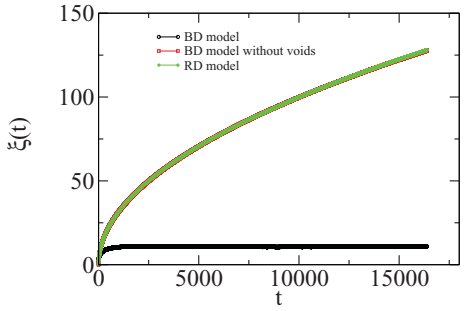

FIG. 4. (Color online) Comparison of height fluctuations in the 1D BD model (black circle) and the fluctuations in the actual depths of the corresponding columns generated using the BD algorithm without the voids (red squares). In the same figure we plot height fluctuations in the RD model (green diamonds). We note that the "depth" fluctuation in the BD model does not saturate and is identical to the height fluctuation in the RD model.

columns generated in the BD model. The effective height of each column as measured by a TEM should be the total number of particles in each column without the voids. Realizing that voids are the result of the sticking rules, one then asks if the correlations are gone when we measure the effective heights without the voids (depths). We have done this exercise while doing BD simulation and measured the effective height of each column. This is shown in Fig. 4. We note that the fluctuations for the effective "depth" without the voids scale as $\xi \sim t^{1/2}$. It will be interesting to test this result by measuring the morphology obtained from BD along the direction of deposition.

C. Slippery BD model and growth from a single site

We now report patterns that we obtain for BD growth from a single site residing either on a flat line (one dimension) or on a surface (two dimensions). This can be viewed as *an extreme limit of growth from a nanocluster.* While looking at growth patterns from a single site we have extended these studies for the SBD model [24,25]. In our studies of SBD we have chosen the probability for adsorption exactly on top of a site to be unity, while the adsorption on other nearest neighbors is determined by a sticking probability p_s. The particles that land at the surface are removed unless they land at a site adjacent to an occupied site. Therefore, an incoming particle might glide by several occupied sites before becoming adsorbed in its final destination, as shown in Fig. 5. We will see shortly that the growth pattern from a single seed is rather insightful. Evidently, having the sticking probability p_s as an additional variable has interesting consequences on the growth pattern.

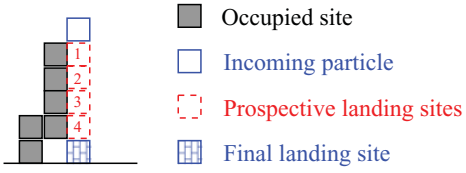

FIG. 5. (Color online) Rendition of the slippery ballistic model. The approaching particle (empty blue square) missed the opportunity to stick at sites 1, 2, 3, and 4 and finally lands at an unoccupied position (hashed blue square).

Lowering the sticking probability results in a denser packing [25,26]. Amar [25] also showed that the fractal dimension of the SBD in the bulk undergoes a discontinuous change as a function of p_s. In the following subsections we show the growth from a single seed in 1D SBD. In addition, we have also looked at the case where we fix the lateral probability p_l for sticking to an adjacent occupied site at the base to be unity. This provides another dimension to control the patterns.

Figure 6 shows snapshots of the growth pattern from a single seed as a function of different sticking probability p_s *from a single simulation*. One immediately notices that (1) in general the patterns grow in the form of a cone and (2) the angle subtended by the cone is a function of the sticking probability p_s. Evidently the angle is maximum for $p_s = 1.0$ and decreases as one lowers the sticking probability. These conclusions are strengthened by looking at the patterns by superimposing growth morphologies from 100 individual simulations, as shown in Fig. 7. These patterns are not only reproducible but can also be well controlled to generate a cone with a particular angle once we know the dependence of this angle as a function of p_s.

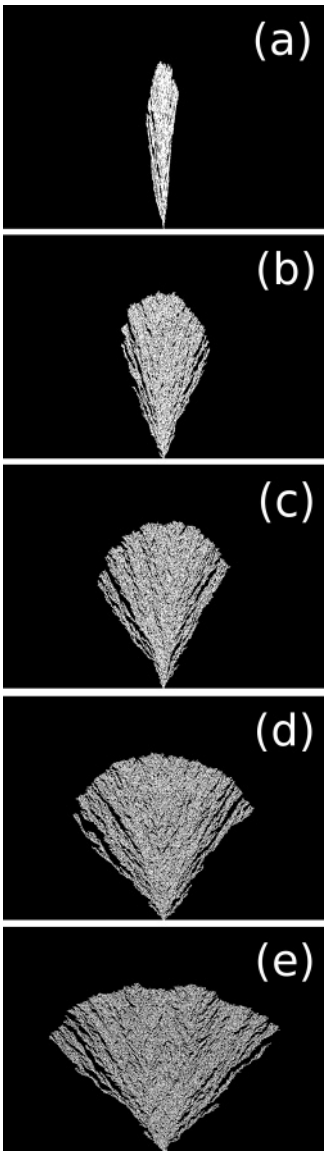

FIG. 6. (Color online) 1D ballistic growth from a single site for various sticking probabilities: (a) $p_s = 0.01$, (b) $p_s = 0.1$, (c) $p_s = 0.25$, (d) $p_s = 0.50$, and (e) $p_s = 1.0$.

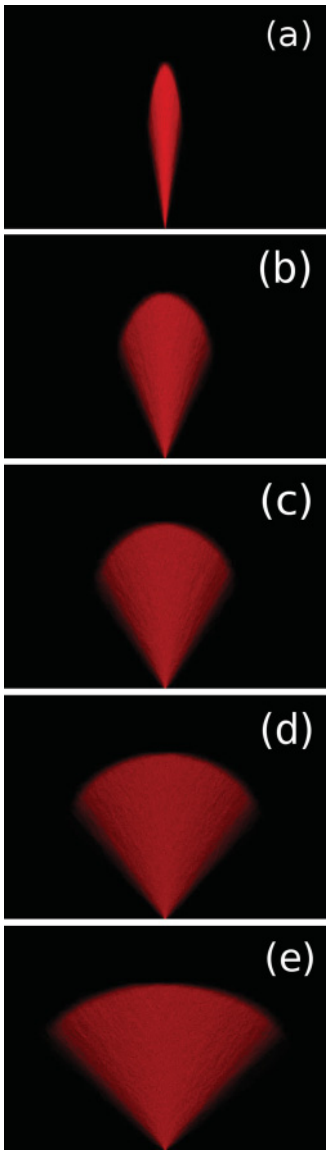

FIG. 7. (Color online) 1D ballistic growth from a single site for various sticking probabilities: (a) $p_s = 0.01$, (b) $p_s = 0.1$, (c) $p_s = 0.25$, (d) $p_s = 0.50$, and (e) $p_s = 1.0$. These snapshots are obtained by superimposing 100 patterns.

To facilitate the discussion that follows we characterize these cone-shaped structures by their average height $\langle h \rangle$ and average width $\langle w \rangle$ [27] and define the angle of elevation θ with respect to the horizontal axis as shown in Fig. 8. The half angle subtended by the cone is ϕ. We further observe that for each sticking probability p_s, the elevation angle θ is not strictly a constant but a weak function of the width $\langle w \rangle$. Its concave shape is depicted by the dotted blue line in Fig. 8.

The more quantitative aspects of the patterns generated are shown in Fig. 9, which shows the average height $\langle h \rangle$ as a function of the average width $\langle w \rangle$ for several values of p_s. This is nothing but the envelope or edge of the cones shown

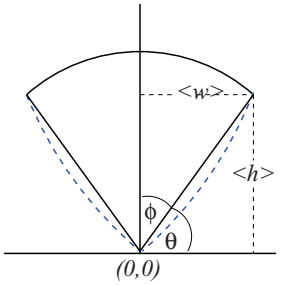

FIG. 8. (Color online) Definitions of width $\langle w \rangle$, height $\langle h \rangle$, and the angle θ subtended by the cone for 1D SBD model. The angle $\theta \to 90^0$ when $p_s \to 0$ and saturates at $\theta \simeq 57^0$ as $p_s \to 1$.

in Fig. 6(a)–6(e) or Fig. 7(a)–7(e). We notice that at an early time the cone is slightly narrower than it is at late time, and the broadening of the cone reflects that saturation of the angle at a long time as seen in Fig. 9. The inset shows these asymptotic values of the cone angles for different p_s. Obviously, when $p_s \to 0$, there is no deposition, and hence the angle $\theta \to 90^\circ$. But for $p_s = 1.0$ the cone angle saturates at $\theta \approx 57^\circ$.

D. Initial and asymptotic angle subtended by the cone

In the following we provide an approximate derivation for the evolution of the angle from its early time value to its saturation value at late time. For simplicity we set $p_l = 0$ and $p_s = 1$ for this discussion. For a given realization we define the angle of growth as $\theta = \tan^1(h/w)$, where h and w are the instantaneous height and width measured with respect to the position of the initial seed. Let us consider the growth from a seed for $p_s = 1.0$. As shown in Fig. 10 only at $t = 2$ does one see the lateral growth. It is obvious that at $t = 1$ the angle $\theta = 45^\circ$ as configurations (b) and (c) occurs with equal probability at $t = 2$. For $t = 3$ we show all the patterns that would result with equal probability starting from each of the three patterns at $t = 2$. In this case the possible angles are $\tan^{-1}(0)$, $\tan^{-1}(2)$, $\tan^{-1}(1)$, and $\tan^{-1}(1/2)$, whose weights can be readily calculated from all the configurations shown in Fig. 10. For example, the weighted probability of occurrence

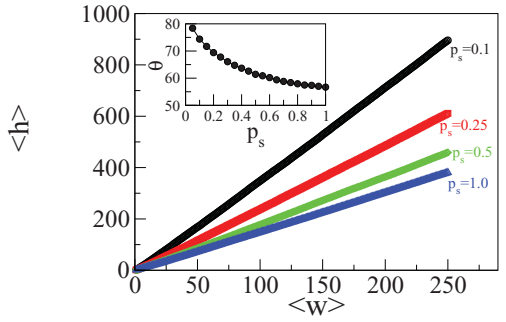

FIG. 9. (Color online) Variation of mean height $\langle h \rangle$ as a function of the mean width $\langle w \rangle$ for 1D SBD for different sticking probabilities p_s. The black circles, red squares, green diamonds, and blue triangles correspond to $p_s = 0.10, 0.25, 0.50$, and 1.00, respectively. The inset shows the variation of the angle $\theta = \tan^{-1}\left(\frac{\langle h \rangle}{\langle w \rangle}\right)$ subtended by the cone as a function of the sticking probability p_s.

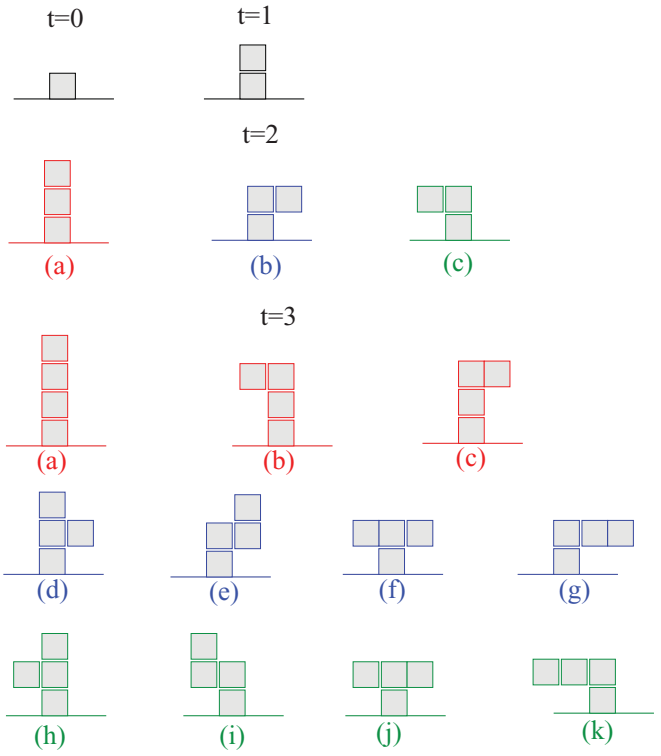

FIG. 10. (Color online) Ballistic growth from a seed. Different options are shown for $t = 1,2$, and 3. Each color in $t = 2$ and 3 should be connected to the corresponding parent configuration.

of $\tan^{-1}(2)$ is

$$\tfrac{1}{3}\left(\tfrac{1}{3} + \tfrac{1}{3}\right) + \tfrac{1}{3}\left(\tfrac{1}{4} + \tfrac{1}{4}\right).$$

Here the factor $1/3$ before each set of parentheses comes from the equal probability of each pattern of $t = 2$ stage to occur. Then for $t = 3$ the patterns (b) and (c), which correspond to the angle $\tan^{-1}(2)$, each occur with $1/3$ probability. Likewise patterns (e) and (i) occur with $1/4$ probability. If we collect all the weights for all the angles, it is very easy to check that the average angle $\langle \theta \rangle$ is given by

$$\langle \theta \rangle = \tfrac{7}{18}\tan^{-1}(2) + \tfrac{1}{3}\tan^{-1}(1) + \tfrac{1}{6}\tan^{-1}(1/2) \simeq 45^\circ. \quad (5)$$

Therefore, at early time for $p_s = 1$ the initial angle of growth is 45°, which is consistent with the simulation.

For larger horizontal distances, the angle of growth is greater than 45° because as the structure grows, there are more chances for the overall height to increase than the overall width. Interestingly, as the horizontal width approaches infinity, the growth angle converges quickly to 57°, as shown in Fig. 11. For $p_s < 1$ from Fig. 10 one notices that the pattern has a higher chance of growing when the particle is deposited on top of a filled site. Therefore in general the asymptotic angle becomes less than 57°.

E. Nanoscaffolds using SBD from seeds

One immediately notices from Figs. 6 and 7 that the structures from a single seed could be exploited by placing the seeds in a periodic array as shown in Fig. 12. By adjusting the periodicity and the sticking probability, a variety of cone-shaped structures are possible. One can imagine that

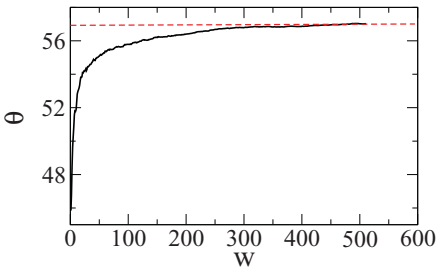

FIG. 11. (Color online) Variation of the angle as a function of the growing width for $p_s = 1.0$.

with the tip of an AFM one can design the periodic array. Irreversible growth with certain sticking probability needs to be designed with appropriate chemistry. Figure 6 shows the results from a single simulation of seed-nucleated growth, for which the edges are rough, as might be anticipated. However, if one superimposes results from multiple simulations, the bounding surfaces become smooth, as in Fig. 7. This implies that suitable processing conditions, e.g., chemical etching, might be used to remove edge roughness subsequent to deposition. It is worth mentioning that possibilities are not restricted to cones only. For example, one can put atomic pillars with certain symmetry and periodicity between two closely placed parallel plates and generate patterns. With imagination, a variety of scaffolds could be generated. Figure 13 shows some images that give a better idea of how different scaffolds could be constructed. Such possibilities are worthy of experimental investigations.

F. Influence of sticking probability at the base

Finally, we would like to cite some examples where we choose the lateral sticking probability at the base to be different from p_s [28]. As an extreme case, we have studied the patterns as a function of p_s by setting $p_l = 1.0$ as shown in Fig. 14. These patterns should be contrasted with patterns in Fig. 7,

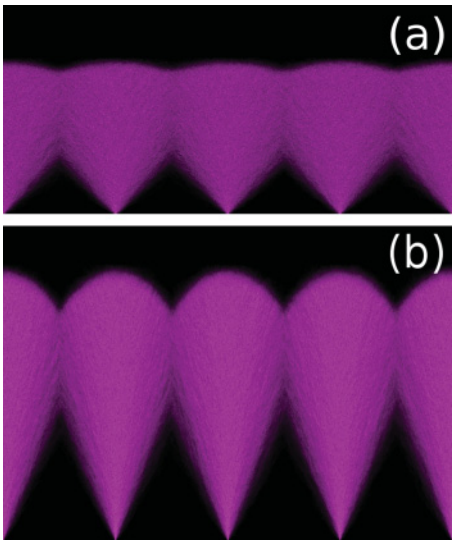

FIG. 12. (Color online) Illustration of how different morphologies could be obtained by adjusting the sticking probability in SBD onto nanoparticle arrays.

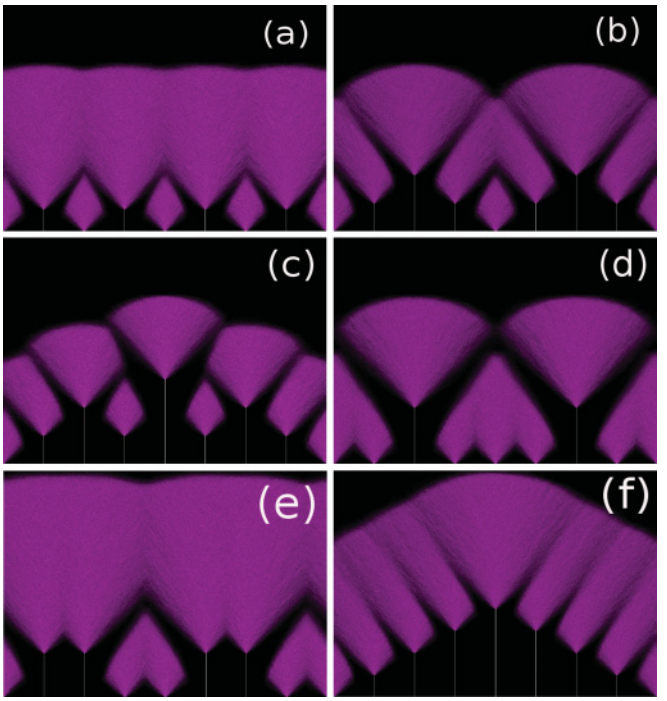

FIG. 13. (Color online) Patterns resulting from 1D SBD model using various values of p_s and distances between nucleation sites.

which were generated setting $p_l = 0.0$. When $p_l = 1.0$, a lower p_s produces a wider pattern at an earlier time. Naturally, a variety of other patterns can be constructed by suitable ratio of p_s/p_l.

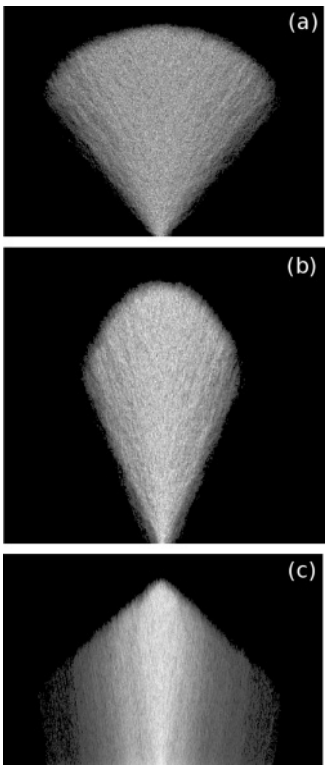

FIG. 14. (Color online) Variation of the shape as a function of different p_s when the lateral sticking probability $p_l = 1.0$; (a) $p_s = 0.5$, (b) $p_s = 0.1$, and (c) $p_s = 0.01$.

G. 2D growth from periodic and randomly placed clusters

We now present preliminary results of an extension of these ideas in two dimensions. Motivated by experiments where deposition occurs from gold nanoclusters (Au-NP), we have extended our studies for growth from nanoclusters. The rules are the same as above so that the empty sites of the surface desorbs completely. 3D surface morphologies at different times are shown in Fig. 15 for a 64×64 lattice. According to the rule the lateral growth at early time is still guided by the growth pattern from a single site. Depending upon the density of the nanoparticles the lateral extension from each cluster eventually coalesces, and soon after that the morphology grows in a similar fashion as that in the bulk. This is nicely captured in the surface density variation as a function of the distance from the plane for several different densities of the seed in Fig. 16. We have checked that for all the densities of the initial seeds the asymptotic density is the same as that of the corresponding bulk system. But for lower density of the seeds it takes longer to reach this asymptotic limit. Therefore, it is profitable to use a uniform flat plane with the entire plane having the same sticking probability to avoid voids that might cause undue instability of the structure grown this way. On the contrary, if one wants to generate rough surfaces with a specific density by SBD, then the empirical curves shown in Fig. 16 could be used to guide the design. These simulated structures are qualitatively similar to what has been observed in vapor-deposited thin films [29].

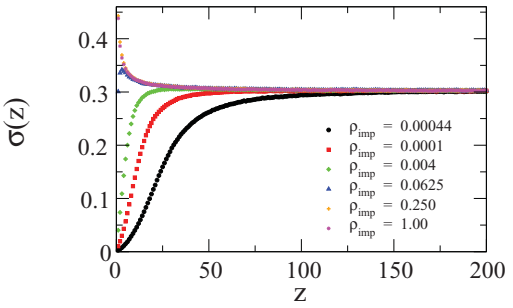

FIG. 16. (Color online) Variation of surface density $\sigma(z)$ as a function of distance z from the origin for several values of the density of the impurity sites. Black circles, red squares, green diamonds, blue triangles, orange plus, and magenta stars represent $\rho_{\text{imp}} = 0.00004$, $\rho_{\text{imp}} = 0.0001$, $\rho_{\text{imp}} = 0.004$, $\rho_{\text{imp}} = 0.0625$, $\rho_{\text{imp}} = 0.25$, and $\rho_{\text{imp}} = 1.0$ (bulk), respectively. Notice that each curve asymptotically approaches the same (bulk) density.

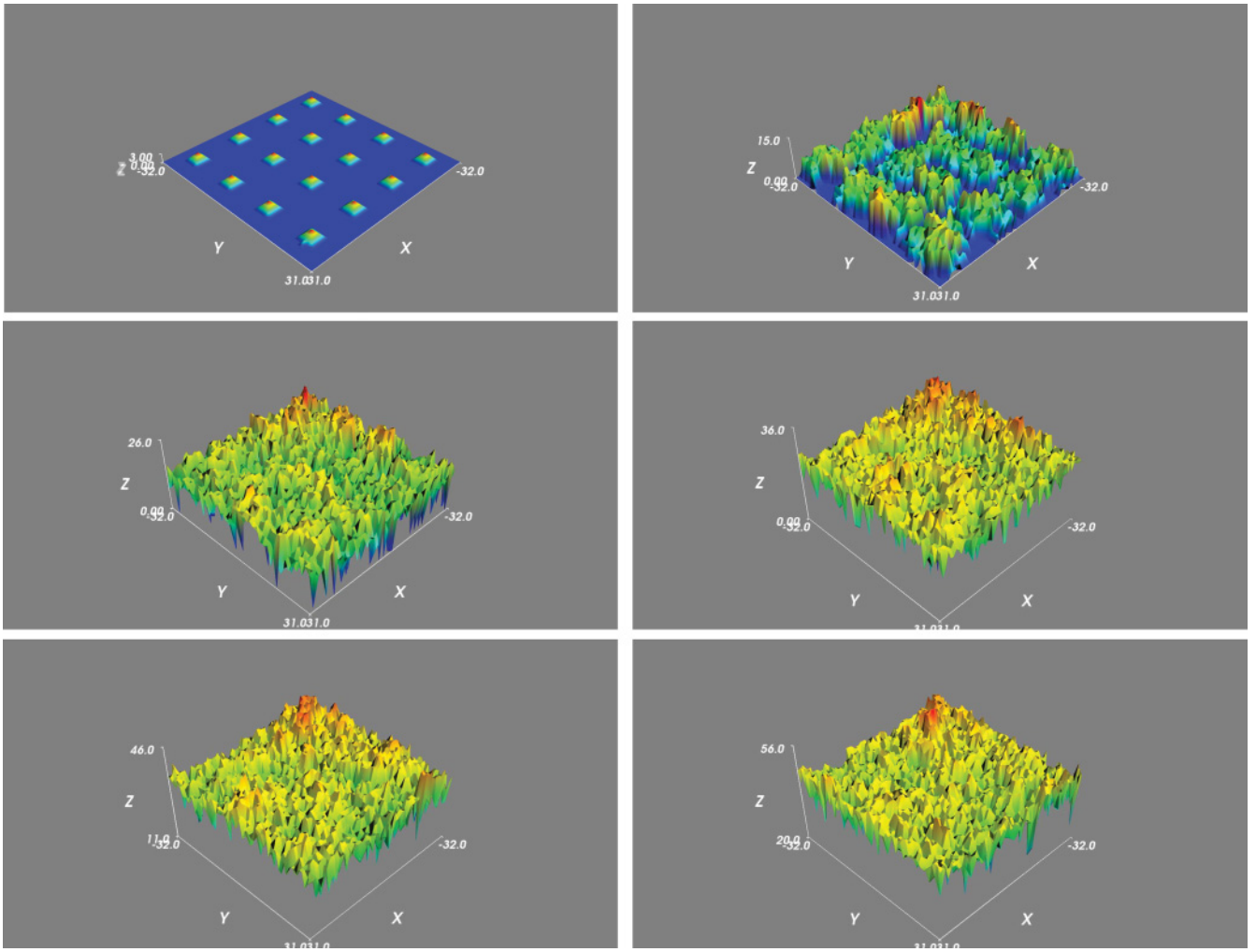

FIG. 15. (Color online) 2D ballistic growth on a flat surface having uniformly distributed seed particles. The corresponding density variation as a function of the vertical distance is shown in Fig. 16.

IV. DISCUSSION AND CONCLUSION

In summary, we have studied some aspects of the regular BD model and many aspects of the growth morphologies from a slippery BD model, in particular, when growth germinates from a single seed particle. By taking simulation runs deep inside the saturation regime for large lattices we easily verified that BD model exponents are the same as that of the KPZ class. Motivated by experimental efforts to investigate the heterogeneities in the morphologies produced by the BD model we then compared the height fluctuations generated by the BD and its corresponding lattice without the voids. We find that the fluctuation in the dual lattice without the voids is the same as that of the RD model. We conclude that the morphology obtained by TEM should not be able to capture the BD features. Here we have studied BD growth using the "slippery BD model," first from a single site and then from periodic sites in one dimension. We observed that as a function of the sticking probability and the length of the periodic lattice one can generate a variety of structures. We then cited a few examples to demonstrate the prospective application of this growth phenomenon to design scaffolds of various kinds. We extended these studies of growth from a periodic lattice in one to two dimensions using the BD scheme. We noted that eventually the surface density of the evolving morphology reaches its bulk counterpart. This method can be used to design a material with a particular surface coverage.

Finally, we also furnished some results where we chose the lateral sticking probability at the base p_l to be unity and studied the evolving morphologies as a function of various p_s. We noted that both early and late time patterns can be controlled by suitable tuning of the ratio p_s/p_l. It is conceivable that some ratios of p_s/p_l may reveal more results. Various structures that can be generated using SBD model in two dimensions from a single site as well as from a variety of Bravais lattices will also be worthy of further investigation. It is worth noting that compared to the regular BD model the SBD model has been studied less extensively. Yu and Amar [25] have reported interesting phase transitions as a function of the sticking probability in some versions of the SBD model. How this will affect the morphologies from a single seed or a periodic array is an interesting issue to investigate. In addition, the effect of the underlying lattice structure, such as a triangular or a honeycomb lattice, on the morphologies grown using the SBD model for various sticking probabilities may reveal interesting results.

ACKNOWLEDGMENTS

The work has been supported by a grant from the National Science Foundation, Chemistry division under Grant No. NSF-CHE 0809821. AR has been partially supported by UCF office of research and commercialization with a matching fund for undergraduate research. AB and AR thank Sumnatha Pattanaik for various discussion about animations and generating colored figures. AR thanks Arup Guha for help with algorithm development in C. AB thanks Tapio Ala-Nissila for comments on the manuscript. We also thank both referees for their constructive comments.

[1] A.-L. Barabasi and H. E. Stanley, *Fractal Concepts in Surface Growth* (Cambridge University Press, New York, 1995).
[2] M. Kardar, G. Parisi, and Y.-C. Zhang, Phys. Rev. Lett. **56**, 889 (1986).
[3] M. C. Cross and P. C. Hohenberg, Rev. Mod. Phys. **65**, 851 (1993).
[4] T. A. Witten and L. M. Sander, Phys. Rev. Lett. **47**, 1400 (1981).
[5] *Proceedings of the Fourth Berkeley Symposium on Mathematical Statistics and Probability, Berkeley, California*, edited by F. Neyman (University of California, Berkeley, 1961), Vol. 4, p. 223.
[6] J. Feder, J. Theor. Biol. **87**, 237 (1980).
[7] M. J. Vold, J. Coll. Sci **14**, 168 (1959).
[8] D. N. Sutherland, J. Coll. Sci **22**, 300 (1966).
[9] P. Meakin, Phys. Rep. **235**, 189 (1993).
[10] T. Halpin-Healy and Y. Zhang, Phys. Rep. **254**, 215 (1995).
[11] Y. S. Chen, A. Tal, and S. M. Kuebler, Chem. Mater. **19**, 3858 (2007).
[12] A. J. Bray, Adv. Phys. **43**, 357 (1994).
[13] F. Family and T. Vicsek, J. Phys. A: Math. Gen. **18**, L75 (1985).
[14] P. Meakin, P. Ramanlal, L. M. Sander, and R. C. Ball, Phys. Rev. A **34**, 5091 (1986).
[15] R. Miranda, M. Ramos, and A. Cadilhe, Comp. Mat. Sc. **27**, 224 (2003).
[16] R. M. D'Souza, Int. J. Mod. Phys. C **8**, 941 (1997).
[17] R. M. D'Souza, Y. Bar-Yam, and M. Kardar, Phys. Rev. E **57**, 5044 (1998).
[18] F. D. A. Aarao Reis, Phys. Rev. E **63**, 056116 (2001).
[19] F. D. A. Aarao Reis, Phys. Rev. E **69**, 021610 (2004).
[20] C. A. Haselwandter and D. D. Vvedensky, Phys. Rev. E **73**, 040101(R) (2006).
[21] F. A. Silveira and F. D. A. Aarao Reis, Phys. Rev. E **75**, 061608 (2007).
[22] H. F. El-Nashar and H. A. Cerdeira, Phys. Rev. E **61**, 6149 (2000).
[23] H. F. El-Nashar, W. Wang, and H. A. Cerdeira, Surf. Sci. **391**, 1 (1997).
[24] R. S. Sinkovits, Physica A **209**, 1 (1994).
[25] J. Yu and J. G. Amar, Phys. Rev. E **65**, 060601 (2002).
[26] R. Julien and P. Meakin, J. Phys. A: Math. Gen. **22**, L1115 (1989).
[27] Here the average width of the cone $\langle w \rangle$ should not be confused with the discussion about the "width" of an growing interface in the context of BD model alluded in Sec. II.
[28] We are indebted to one of the referees for bringing this point to our attention.
[29] R. Messier and J. E. Yehoda, J. Appl. Phys. **58**, 3739 (1985).